Boundary-Layer Meteorology (2005) 114: 53–70

ATMOSPHERIC BOUNDARY-LAYER STRUCTURE OBSERVED DURING A HAZE EVENT DUE TO FOREST-FIRE SMOKE

MARKUS PAHLOW[1,*], JAN KLEISSL[1], MARC B. PARLANGE[1], JOHN M. ONDOV[2] and DAVID HARRISON[2]

[1]*Department of Geography and Environmental Engineering, and Center for Environmental and Applied Fluid Mechanics, Johns Hopkins University, Baltimore, MD 21218, U.S.A.;*
[2]*Department of Chemistry and Biochemistry, University of Maryland, College Park, MD 20742, U.S.A.*

(Received in final form 23 March 2004)

Abstract. During a haze event in Baltimore, U.S.A. from July 6 to 8, 2002, smoke from forest fires in the Québec region (Canada), degraded air quality and impacted upon local climate, decreasing solar radiation and air temperature. The smoke particles in and above the atmospheric boundary layer (ABL) served as a tracer and provided a unique opportunity to investigate the ABL structure, especially entrainment. Elastic backscatter lidar measurements taken during the haze event distinctly reveal the downward sweeps (or wisps) of smoke-laden air from the free atmosphere into the ABL. Visualisations of mechanisms such as dry convection, the entrainment process, detrainment, coherent entrainment structures, and mixing inside the ABL, are presented. Thermals overshooting at the ABL top are shown to create disturbances in the form of gravity waves in the free atmosphere aloft, as evidenced by a corresponding ripple structure at the bottom of the smoke layer. Lidar data, aerosol ground-based measurements and supporting meteorological data are used to link free atmosphere, mixed-layer and ground-level aerosols. During the peak period of the haze event (July 7, 2002), the correlation between time series of elastic backscatter lidar data within the mixed layer and the scattering coefficient from a nephelometer at ground level was found to be high ($R = 0.96$ for $z = 324$ m, and $R = 0.89$ for $z = 504$ m). Ground-level aerosol concentration was at a maximum about 2 h after the smoke layer intersected with the growing ABL, confirming that the wisps do not initially reach the ground.

Keywords: Atmospheric boundary layer, Baltimore PM Supersite, Entrainment, Forest fire, Haze event, Lidar.

1. Introduction

As with all particulate air pollution, forest fire smoke impacts upon local visibility and air quality, leading to health risks for the exposed population. The negative effects are often not restricted to the immediate environment, however. Hot gases and particles from the fires rise into the atmosphere, often reaching the free troposphere or stratosphere. Large-scale advective transport of this gas/particle mixture can then affect air quality in locations remote from

* Present address: NOAA, Environmental Technology Laboratory, Boulder, CO 80305, U.S.A. E-mail: markus.pahlow@noaa.gov

the fire itself (e.g., Wotawa and Trainer, 2000; Forster et al., 2001). These forest fires are occasionally caused by human activity, but most (approximately 85%) are caused by lightning (Weber and Stocks, 1998). Episodically, organic carbon (OC) emissions from boreal fires are the dominant source of regional levels of OC for the eastern and south-eastern United States, a region with one of the highest anthropogenic emission rates worldwide (Wotawa and Trainer, 2000). Transport of forest fire plumes originating in Canada towards the United States is not uncommon (Skinner et al., 1999). Furthermore, the annual average area of burned forest has more than doubled since the 1970s (Skinner et al., 2002). By the first week of July 2002, fires in the Québec region had consumed some 162,000 ha of forest, twice as much as the annual average.

It is often due to large-scale subsidence that the aerosol from the forest fires is forced down to low altitudes, after it has been advected horizontally with the prevailing winds (Iziomon and Lohmann, 2003). If so, the smoke-laden air from higher altitudes is likely to intersect the atmospheric boundary layer (ABL), and thereafter a type of 'fumigation' process distributes the gases and aerosols within the turbulent ABL. The haze event in Baltimore from July 6 to 8, 2002, resulted in the strong impact of combustion products such as black carbon, organic carbon and $PM_{2.5}$ (particulate matter with an aerodynamic diameter ≤ 2.5 μm) on a region remote from the fire origin. Events such as this emphasise the importance of improving our understanding of gas and aerosol transport into the ABL from aloft, particularly because smoke aerosols can affect health, surface temperature (Robock, 1988a, b) and regional climate (Menon et al., 2002).

There is a long observational history of studies that examine ABL structure and time evolution. Different techniques and a variety of instrumentation probing the ABL, have been employed in the field (see references in Stull (1988) and Garratt (1992), and more recently e.g., Angevine et al. (1998a), Menut et al. (1999) and Yi et al. (2001)). Laboratory experiments have helped to further our understanding on distinct processes (e.g., Deardorff et al., 1980; Fedorovich and Thäter, 2002), while large-eddy simulation has also been used to study specific ABL processes in great detail (e.g., Wyngaard and Brost, 1984; Sullivan et al., 1998; Albertson and Parlange, 1999).

Here we present results from an experimental study in Baltimore, MD in the U.S.A. where smoke from forest fires in Québec was entrained into the ABL from aloft. The goal of this particular investigation is to provide a detailed description of the boundary-layer structure during the haze event and to link ABL processes with meteorological conditions and aerosol concentration at ground level. A comparison is made between the relatively clean atmosphere on July 6, the heavily polluted conditions on July 7, and the aftermath on July 8, which was characterised by a slow cleansing process. Most of the observations presented in this paper are from the Johns Hopkins University (JHU)

lidar supported by ground-based point sensors to characterise aerosol size and composition, as well as data from a micrometeorological station.

2. Experiment

Particulate matter (PM) Supersites is an ambient monitoring research program, funded by the U.S. Environmental Protection Agency (EPA). The program addresses the scientific uncertainties associated with fine particulate matter. The programs of the eight PM Supersites, operated during 1999–2003 around the United States, focus on fine particulate characterisation, methods testing, and support to health effects and exposure studies. Observations taken in the context of the Supersite project in Baltimore are intended to provide an extended, highly time, size, and compositionally resolved dataset, including an indicator of cardiopulmonary response in support of testing hypotheses relating to source attribution and health effects of PM.

Here we report on observations made at the Ponca St. sampling site in downtown Baltimore (39°17′20″ N, 76°33′16″ W, elevation approximately 40 m above sea level), during a haze event caused by forest fires in Québec, Canada, from July 6 to 8, 2002. To characterise atmospheric boundary-layer dynamics, meteorological conditions and atmospheric aerosols, data obtained with the following instruments are analysed. The JHU elastic backscatter lidar system (see Pahlow (2002) for a full system description), a micrometeorological tower, an integrating nephelometer operating at 530 nm (Radiance Research Model M-903), a tapered element oscillating microbalance (TEOM) and a semi-continuous elemental and organic carbon (EC/OC) monitor, the latter three all mounted at a height $z = 3.5$ m.

The lidar system was operated at 1064 nm in upward pointing mode at ground level, with a time resolution of 5 s and a range resolution of 3.75 m. The micrometeorological tower was instrumented with a pyranometer ($z = 11.0$ m), a wind vane ($z = 10.4$ m), two cup anemometers ($z = 5.8$ and 10.4 m), a hygrometer ($z = 4.9$ m), a rain gauge ($z = 3.0$ m) and a pressure sensor ($z = 2.5$ m). Micrometeorological and nephelometer data were recorded as 5-min averages. The TEOM provided fine particle mass concentration, integrated over 30-min intervals, and the elemental and organic carbon monitor gave data integrated over 1-h periods. Note that local standard time (LST) is used throughout this discussion, which corresponds to eastern daylight time (EDT) for the time period studied here.

3. Canadian Forest Fires: Causes and Consequences

Starting July 2, 2002, some 85 forest fires broke out in two regions south-east of James Bay, central Québec, 350–650 km north of the U.S. border. A

combination of prevailing drought conditions in eastern North America and lightning strikes initiated the fires. Strong winds enhanced fire intensity. The fires, some of them burning out of control, produced large amounts of smoke. The smoke was advected southward to the north-eastern U.S.A. and the Atlantic Ocean as a cyclone intensified over the Canadian Maritimes and reached parts of the mid-Atlantic region, including Maryland and the city of Baltimore, by July 6, 2002. The MODIS satellite image (Figure 1) from July 7, 2002, outlines active forest fires and the pathway of the forest-fire smoke. High pressure subsidence forced the smoke to lower altitudes. Figure 2a shows the time series of atmospheric pressure recorded at the Baltimore PM Supersite during July 6–8, 2002. Northerly winds advected the smoke to Baltimore on July 6 (Figure 2b); weak winds elongated the residence time of smoke in the ABL (Figure 2c). The smoke signature can clearly be seen in the time series of solar radiation (SR) (Figure 2d). The maximum SR on cloud-

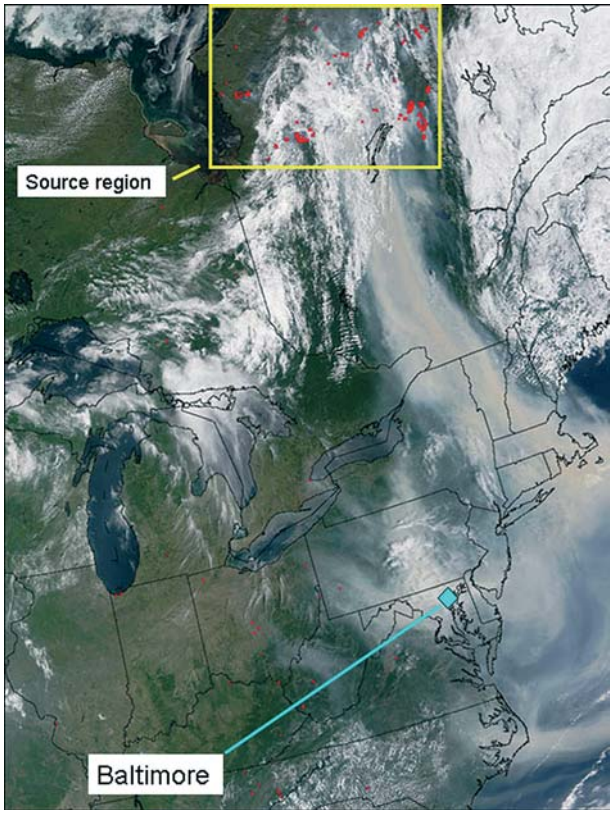

Figure 1. MODIS satellite image taken on July 7, 2002 at 1035 LST. The red dots represent active forest fires. The pathway of the smoke plume from Québec to the eastern United States can clearly be seen. MODIS satellite image courtesy of Land Rapid Response Team, NASA/GSFC, Greenbelt, MD, U.S.A.

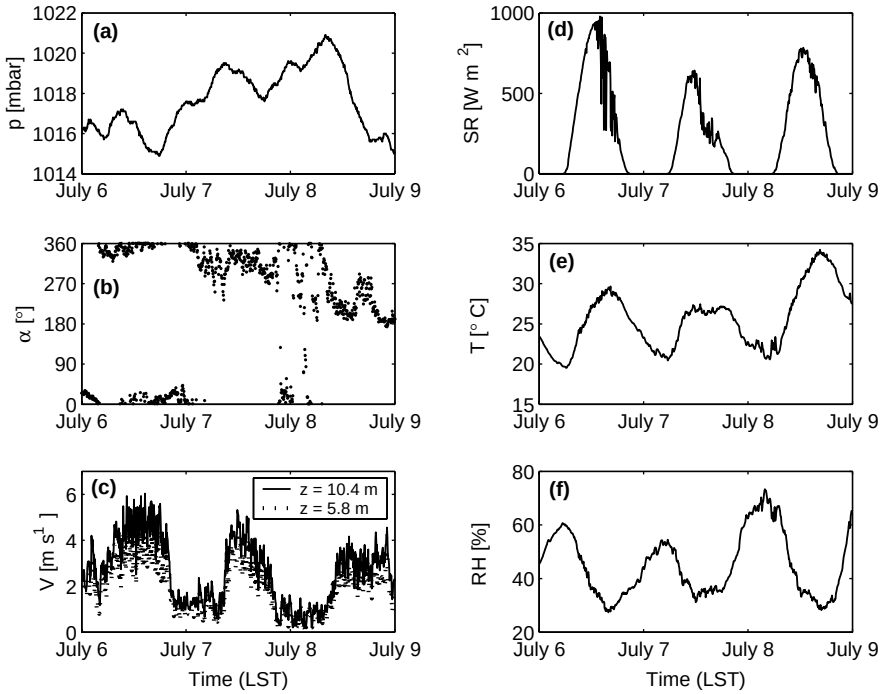

Figure 2. (a) Atmospheric pressure p, (b) wind direction α, (c) horizontal wind speed V measured at two heights, (d) solar radiation SR, (e) air temperature T and (f) relative humidity RH at the Ponca St. field site in Baltimore during July 6–8, 2002. Tick marks along the abscissa axis denote midnight.

free July 7, the peak period of the haze event, is 34% lower than that on July 6, where clouds prevailed in the afternoon, and 18% lower than that on July 8, a day with little cloud cover. This, in turn, affects air temperature (Figure 2e), with a July 7 maximum that is 2.3 °C lower than the maximum on July 6 and 6.8 °C lower than the maximum on July 8. The mean air temperature on July 7 fell 2.8 °C below the monthly mean air temperature. Relative humidity (RH) was low during the forest-fire peak event, about 10–15% below typical July values (Figure 2f); in the early afternoon of July 8, the atmospheric pressure fell. This indicated the approach of a cold front, which, together with a shift in wind direction (Figure 2b), directed the smoke eastward over the Atlantic, ending the haze event.

4. Visibility and Aerosol Properties

To illustrate how the smoke aerosols influenced various parts of the east coast of the U.S.A. in particular Baltimore and the vicinity, we present

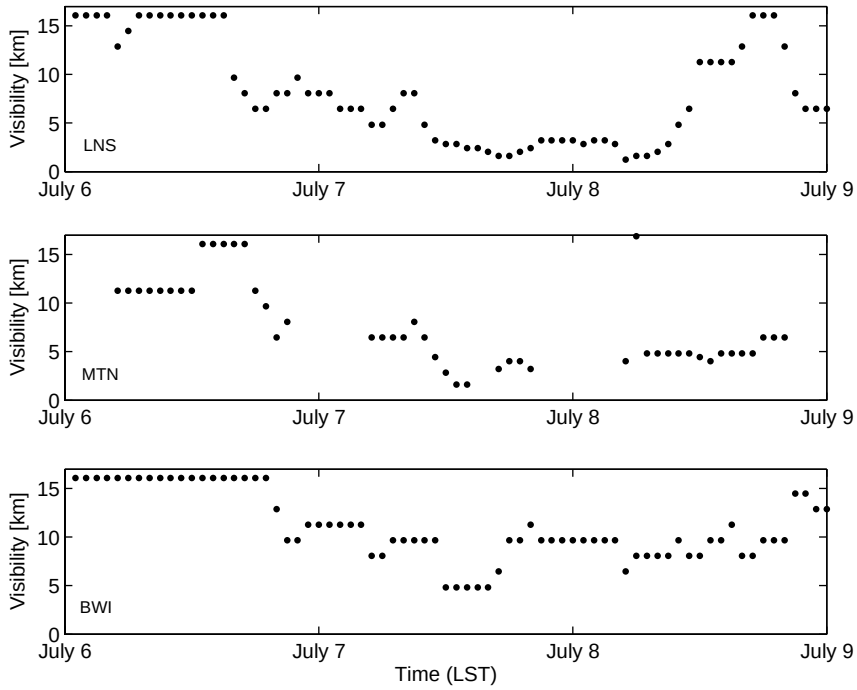

Figure 3. Visibility at three airports (top: LNS, middle: MTN and bottom: BWI) during July 6–8, 2002. The maximum visibility recorded at airports is 16 km. Tick marks along the abscissa axis denote midnight.

visibility measurements at airports in Figure 3. Lancaster airport [(LNS) 40°7′18″ N, 76°17′45″ W] is located 95 km north of Baltimore, Martin State airport [(MTN) 39°19′32″ N, 76°24′49″ W] is 15 km east of Baltimore, and Baltimore–Washington International airport [(BWI) 39°10′31″ N, 76°40′ 6″ W] is 15 km south of Baltimore. Figure 3 clearly shows that visibility is decreased strongly by the forest-fire smoke, and that all three locations are affected, starting in the evening of July 6. The impact of aerosols on visibility over the 3-day period under consideration is strongest at LNS, with a minimum visibility of 1.2 km. At the other two locations the minimum is recorded as 1.6 km at MTN and 4.8 km at BWI, respectively. Therefore, the smoke has been entrained into the ABL over a large area, but the impact differs geographically. This was confirmed by Sigler et al. (2003), who recorded high ground-level pollution concentrations on July 7 near Petersham, MA (540 km north-east of Baltimore) due to the Canadian forest-fire smoke. Note that the visibility at LNS begins to increase again on July 8, after the peak period of the haze event, but falls later on. It remains mostly low at MTN and BWI (with larger values at BWI) during July 7 and 8, which

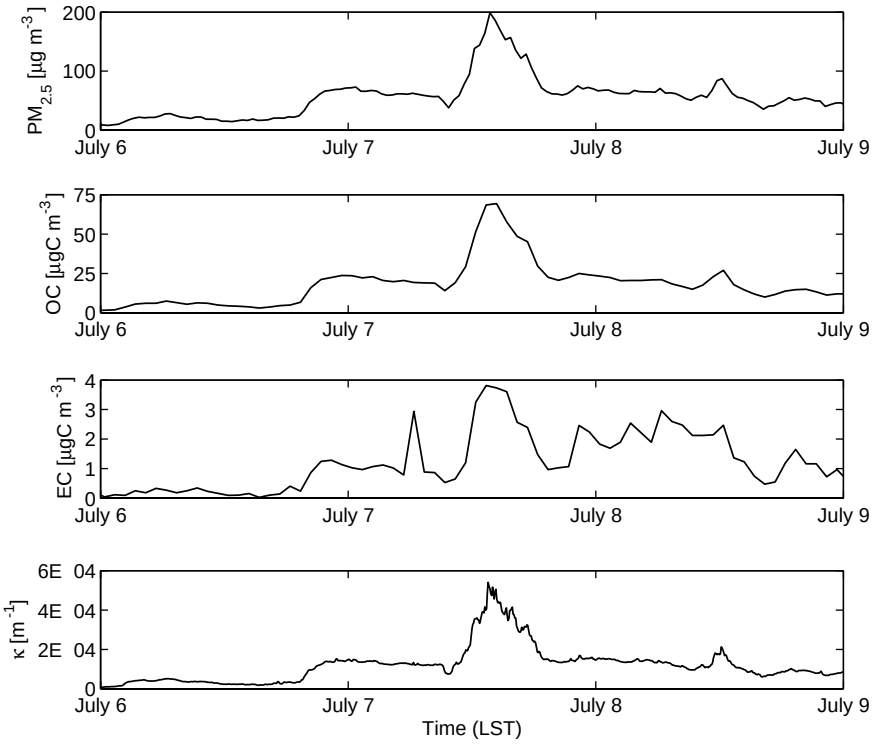

Figure 4. Fine particle (<2.5 μm) mass concentration $PM_{2.5}$, organic carbon OC, elemental carbon EC and scattering coefficient κ for the time period July 6–8, 2002. Tick marks along the abscissa axis denote midnight.

implies that the aerosols were not removed rapidly and that the atmosphere remained turbid.

In order to characterise ground-level aerosol during the haze event, the fine particle mass concentration $PM_{2.5}$, OC, elemental carbon (EC, effectively equivalent to black carbon), and the scattering coefficient κ are shown in Figure 4. These four variables are chosen for specific reasons: the $PM_{2.5}$ measurement yields a clear aerosol particle signature, and both OC and EC are primary forest-fire combustion products, and therefore serve as a tracer for the smoke aerosols caused by the Canadian forest fires. The nephelometer data, which yield the scattering coefficient, are related to the lidar measurements, as both use light scattering as the underlying principle. The effect of smoke particles can clearly be seen in the time series of $PM_{2.5}$ (Figure 4); $PM_{2.5}$ starts to increase in the evening of July 6 (around 1900 LST), indicating the arrival of the forest-fire smoke. The maximum $PM_{2.5}$ occurs in the early afternoon (measurement interval 1315–1345 LST) on July 7 with a value of 198.8 μg m^{-3}, and remains elevated after the maximum value (mean

concentration on July 8, 56.0 μg m^{-3}), compared to the concentration before the haze event (mean concentration on July 6, 29.1 μg m^{-3}). The scattering coefficient and organic carbon are strongly correlated with $PM_{2.5}$, with temporally coinciding maxima ($OC_{max} = 69.4$ μgC m^{-3}, $\kappa_{max} = 5.41 \times 10^{-4}$ m^{-1}), whereas EC increases at times when $PM_{2.5}$ and OC measurements remain comparably low. This is due to the fact that EC is only a signature for certain forest-fire smoke particles. Depending on the type of fire (e.g. fast flaming, smoldering, dry, green, wet) the EC fraction may range from 10% to almost zero.

5. Lidar Observations of the ABL Structure

Time series of boundary-layer height are a good indicator of the strength of convective activity in the ABL, because the surface heat fluxes drive the ABL diurnally. Figure 5 presents the time series of ABL height for July 6–8, 2002, determined from lidar data. The maximum boundary-layer height for July 6 ($z_{i,max} = 1723$ m) and July 8 ($z_{i,max} = 1601$ m) strongly exceeded the maximum ABL height of the peak day of the haze event July 7 ($z_{i,max} = 1164$ m).

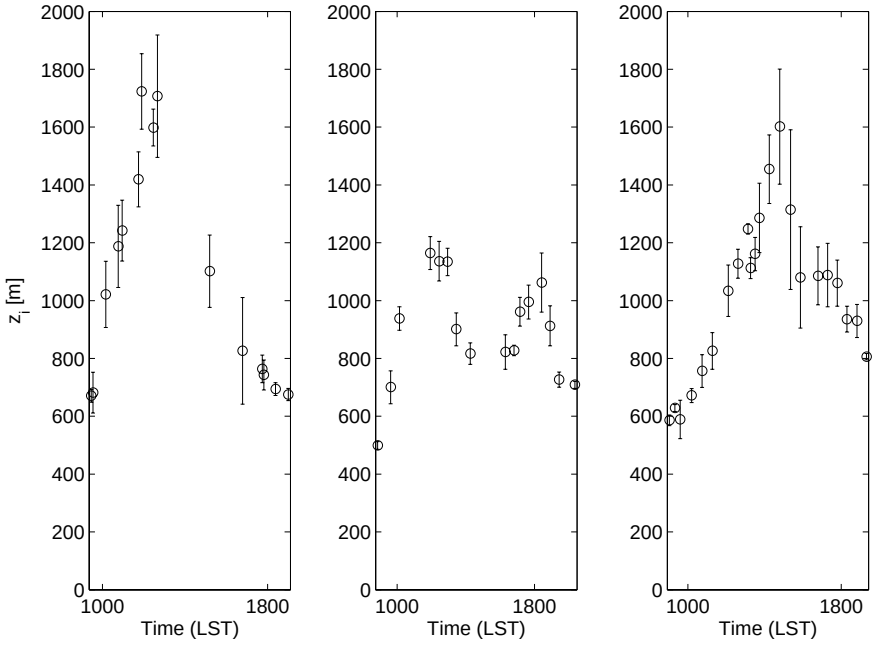

Figure 5. ABL height z_i, as determined from lidar data using a gradient-contour method, for July 6–8, 2002 (July 6: left panel; July 7: middle panel; July 8: right panel). Error bars denote one standard deviation from the mean for each respective time interval.

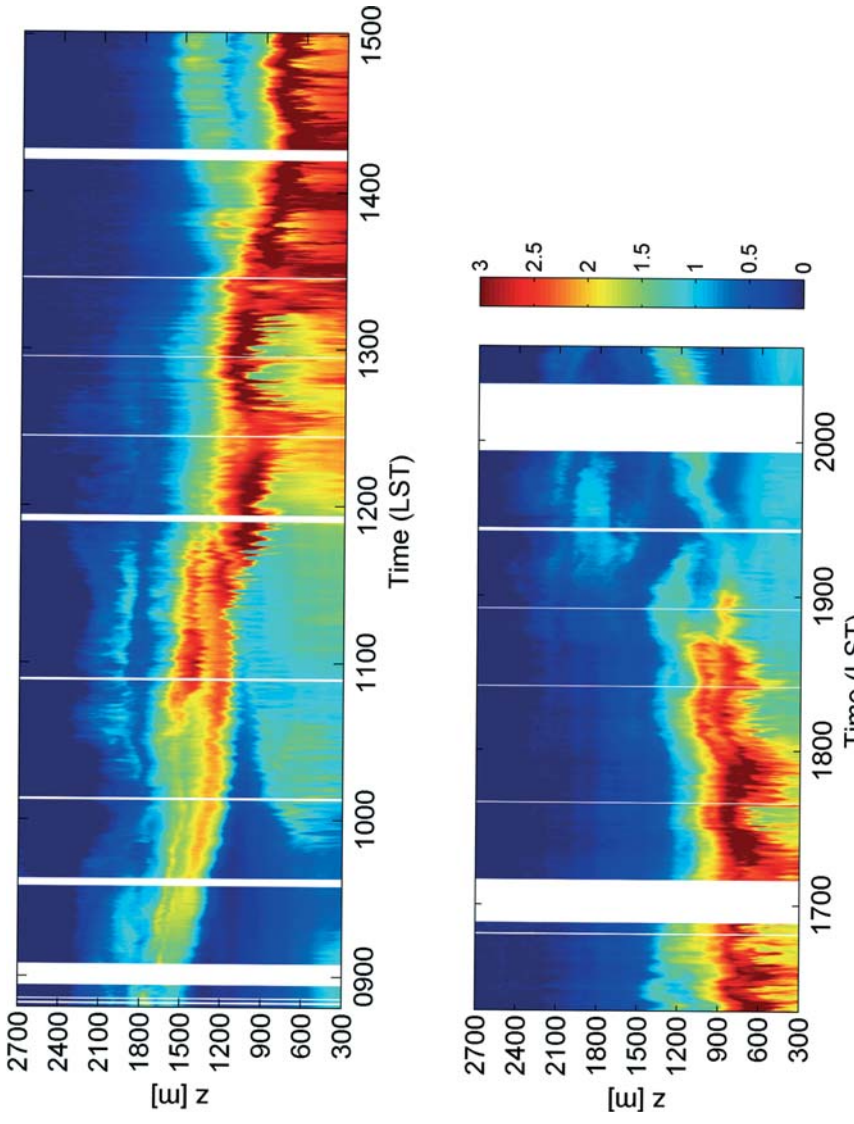

Figure 6. Lidar time series of relative aerosol backscatter from 0847 to 1503 LST (top panel) and from 1618 to 2035 LST (bottom panel).

The forest fire smoke reduced solar heating of the ground (see Figure 2d), which in turn reduced the surface heat fluxes, thus causing reduced convective activity and a lower ABL height.

The smoke particles served as flow tracers and provided an excellent visualisation of boundary-layer processes. The first lidar backscatter data time segment (Figure 6 top panel) from 0847 to 1503 LST shows the coherent layer of forest-fire smoke that is forced down to lower altitudes due to subsidence over the area. Note the coherence of the smoke plume, ranging initially in height from about 1500 to 2250 m. The shallow ($z_i \approx 500$ m) early morning boundary layer is aerosol laden due to rush-hour traffic. Starting at around 0950 LST, the growth of the convective boundary layer (CBL) can clearly be seen, whereas the smoke layer continues to descend to lower altitudes (until around 1100 LST). Note that thermals, overshooting at the boundary-layer top, create a disturbance in the stably stratified layer aloft, which propagates up to the bottom of the smoke layer, manifest in coinciding upward and downward movements of air. The dynamic interaction of the CBL with the free troposphere has been studied previously (e.g., Gossard and Richter, 1970; Metcalf, 1975; Stull, 1976a, b). Recently, Fochesatto et al. (2001), using ground-based lidar, observed dynamic coupling between the growing convective boundary layer and the residual layer. They found that the top of the residual layer started to fluctuate shortly after the CBL began to develop, indicating gravity waves that were excited by overshooting thermals at the top of the CBL.

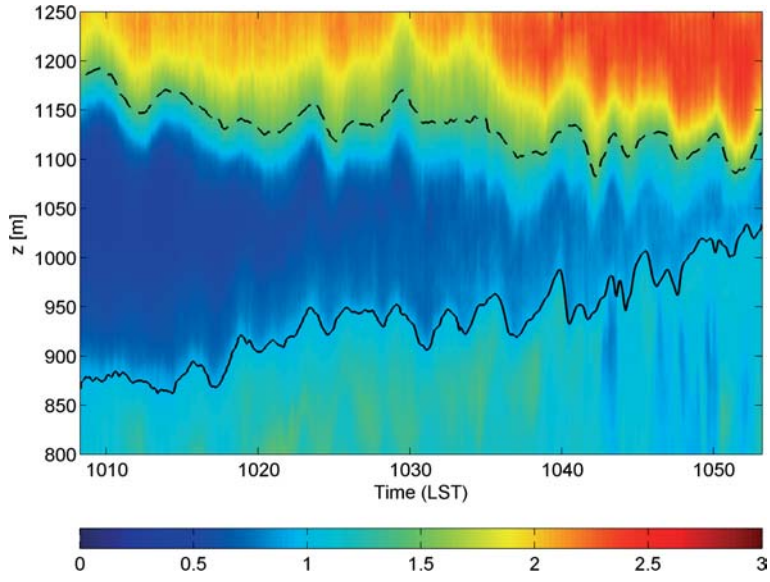

Figure 7. Lidar time series of relative aerosol backscatter from 1008 to 1053 LST. The ABL top and smoke-layer bottom are outlined by the solid and dashed lines, respectively.

Using smoke as a 'tracer', we investigate the interaction between the CBL and the overlying air on July 7. In Figure 7 the lidar time series shows the growth of the CBL and the descending smoke layer aloft between 1008 and 1053 LST. From visual inspection, the growing CBL and the overlying smoke layer appear to be coupled. Domes forming on top of the CBL correspond to the ripple structure at the bottom of the smoke layer. The top of the growing convective boundary layer and the bottom of the forest-fire smoke layer are determined from the lidar backscatter signal using a combined gradient-contour method (solid and dashed lines in Figure 7). To correlate the two time series we subtract their trends and correlate the fluctuations. The correlation coefficient for the time series of fluctuations of ABL top and smoke-layer bottom is largest for a time lag of 25 s, with $R = 0.48$ (for zero time lag: $R = 0.37$). Since the vertical separation between ABL top and smoke-layer bottom ranges from approximately 300 to 60 m, the correlation between the two time series is due to wave motion and not due to coherent turbulent structures. This maximum correlation for a time lag of 25 s is indicative of the group speed of gravity waves excited by thermals at the top of the ABL. From the mean distance between ABL top and smoke-layer bottom of about 200 m, a mean group speed $c_g = (200\ \text{m})/(25\ \text{s}) = 8\ \text{m s}^{-1}$ is determined.

Shortly after 1100 LST the smoke layer and the CBL make contact. The smoke layer atop the CBL serves as a tracer and clearly outlines the thermals overshooting at the boundary-layer top, and the wisps sinking back into the CBL. This interplay is known as penetrative convection (Scorer, 1957; Deardorff et al., 1969; Stull, 1976a). Under regular atmospheric conditions penetrative convection would result in cleansing of the CBL, since downdrafts would carry clean free atmospheric air from aloft into the CBL. From 1140 LST onwards the smoke layer is embedded and confined in the entrainment zone (EZ) due to thermals impinging from the bottom, and due to the stable free atmosphere (FA) above ('lid effect'). Entrainment characteristics of penetrative convection such as dome (due to thermal updrafts, Stull, 1976a) and wisp (downdrafts termed 'wisps' by Deardorff et al., 1969) structures become clearly identifiable throughout the lidar time series. At around 1230 LST, large amounts of aerosol particles are being 'washed downward' through the mixed layer to the ground by means of wisps, about 50 min after the smoke layer becomes embedded in the entrainment zone. Also, from about 1200 LST onward, more aerosols are transported upward from the surface, since the entrainment of smoke has increased the ground-level aerosol concentration by that time (see Figure 4). The downward transport intensifies at around 1315 LST and thereafter. Vigorous downward mixing in either coherent 'sheets' of aerosols or in broad 'curtains' of aerosols continues throughout this time period to further degrade air quality within the mixed layer. Upward and downward transport is almost indiscernible at

this stage. Another process that can be observed is detrainment, the reverse of entrainment (Deardorff et al., 1980). Small pockets of aerosol-laden air detrain from the boundary layer, which can be seen clearly at around 1345 LST. This occurs when overshooting thermals do not sink back into the ABL, but break away and remain in the free atmosphere. Furthermore, detrainment evolves into a process that will be termed 'detachment'. A coherent layer of aerosol-laden air separates from the boundary layer at around 1415 LST, which in turn leads to a decrease of the boundary-layer height. Relatively clear air separates the CBL from the smoke layer aloft. This ABL debris might be re-entrained thereafter or remain in the residual layer or free atmosphere until it becomes re-entrained the following day. Downward mixing of aerosols continues throughout the afternoon, as can be seen in the lidar backscatter data time series (Figure 6, bottom panel) from 1618 to 2035 LST. Interestingly, the smoke layer that was confined in the EZ begins to detach after 1830 LST and the negative impact on air quality lessens. Along with the decreasing convective activity during the evening period, penetrative convection ceases. In addition, the inversion at the ABL top weakens during the transition from daytime, through evening, to nighttime. Hence the smoke layer, formerly trapped in the entrainment zone, disconnects and is advected by the large-scale outer flow (see Figure 6, bottom panel). In the process, the layer spreads out and the smoke aerosol remains as debris in the residual layer, up to an altitude of about 2400 m. However, a coherent layer is lifted off by large-scale motion (near 1930 LST), undergoing upward transport and at the same time the stable nocturnal boundary layer starts to form.

6. Linking ABL and Ground-Level Observations

Due to the zone of incomplete overlap between the laser beam and the field of view of the telescope, a vertically staring lidar can provide information upwards from a certain level only (here $z_{\min} \approx 300$ m). We investigate the possible link between ABL entrainment and mixing, as observed with the lidar, to *in situ* ground-level measurements. Of particular importance is the comparison between remotely sensed lidar data in the mixed layer and data obtained from *in situ* measurements in the atmospheric surface layer. Since the time series of the scattering coefficient on July 7 is representative of the temporal evolution of $PM_{2.5}$, OC, and also of EC during the peak period (see Figure 4), and since κ is available at higher temporal resolution, we use the nephelometer data to compare with relative aerosol backscatter data from the lidar. The lidar and nephelometer serve as a means a to determine the upward (through thermals) and downward (through wisps) transport of aerosols through the surface layer and mixed layer. Concentrations in both

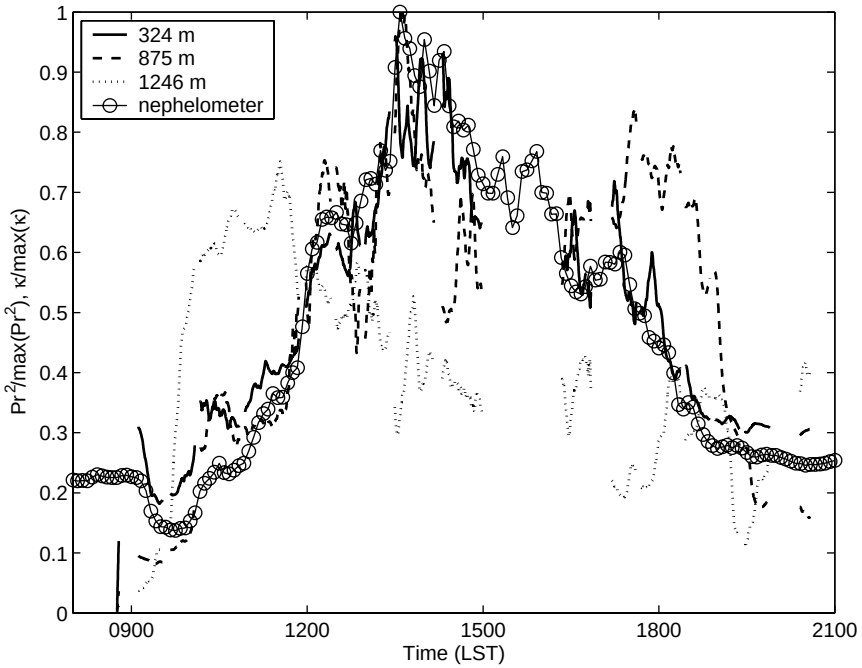

Figure 8. Lidar transects (5-min moving average) at different heights and nephelometer data for July 7, 2002. The lidar (lidar data P corrected with r^2, where r is range from the lidar) and nephelometer data are normalised by their respective maximum values. The levels were chosen to lie always below z_i (level $z = 324$ m), alternating above and below z_i (level $z = 875$ m) and always above z_i (level $z = 1246$ m).

time series are related to the occurrence of these events. Mixing due to turbulence of smaller scales also contributes to a vertical homogenization of the flow, but the mixing due to large scales is dominant in convective conditions. Thorough mixing of smoke aerosols in the whole ABL will increase the lidar backscatter signal throughout, as well as the scattering coefficient of the nephelometer on the ground. Plots of lidar transects (5-min moving average) at several heights, along with the nephelometer data, are presented in Figure 8. For ready comparison, the vertical axis is normalised by the respective maximum value of each measurement. The nephelometer data and lidar data at a certain level correspond well for distinct, yet certainly not all, time periods. The lidar signal at $z = 1246$ m always samples the free atmosphere, since the maximum ABL height is 1164 m. In the morning the lidar signal at $z = 1246$ m samples the smoke layer descent above the ABL and hence is greater than the nephelometer signal. In the afternoon the smoke layer is embedded in the ABL such that the lidar at $z = 1246$ m samples free atmospheric air with smaller smoke concentrations than at the ground. When levels within the ABL are chosen, the correlations are larger and increase

TABLE I

Matrix of correlation coefficient R for lidar transects at several levels (normalised relative aerosol backscatter) and nephelometer 'neph' (normalised scattering coefficient, measured at ground level).

	324 m	504 m	684 m	875 m	1066 m	1246 m	Neph
324 m	1.00	0.94	0.82	0.72	0.51	0.12	0.96
504 m	0.94	1.00	0.88	0.72	0.44	0.09	0.89
684 m	0.82	0.88	1.00	0.74	0.35	0.004	0.81
875 m	0.72	0.72	0.74	1.00	0.63	0.08	0.75
1066 m	0.51	0.44	0.35	0.63	1.00	0.39	0.56
1246 m	0.12	0.09	0.004	0.08	0.39	1.00	0.12
Neph	0.96	0.89	0.81	0.75	0.56	0.12	1.00

Levels z = 324 and 504 m were always below z_i, z = 684, 875 and 1066 m were alternating above and below z_i and z = 1246 m was always above z_i.

with proximity to the ground. The increase in correlation can clearly be seen from Figure 8 for a few selected representative levels. The intermediate height, $z = 875$ m, alternately lies above and below z_i, corresponding to varying agreement with the nephelometer. Between 1800 and 1900 LST the smoke layer lifts, hence the aerosol concentration increases in this height region, and therefore the lower correlation with ground-level observations. The height $z = 324$ m lies always within the ABL during the time period under consideration and exhibits a strong correlation between lidar and nephelometer ($R = 0.96$). The data correlate best for zero time lag. Table I summarises the comparison between lidar and nephelometer in the form of a correlation matrix. The high correlation coefficient R between the lidar at 324 m and nephelometer suggests strong coupling of the lower mixed layer and near surface air pollution levels for time scales >5 min. Measurements at levels that were always below z_i ($z = 324$ and 504 m) show the highest correlation with each other and with ground-level observations.

Two interesting events, as observed with lidar, were corroborated by nephelometer data. From 0915 to 0950 LST a strong decrease in the lidar signal was recorded at low altitudes (see Figure 6, top panel). This corresponds to a strong decrease in the scattering coefficient measured at the ground (see Figure 8). A possible cause is the reduction of ambient aerosol from car exhaust after the morning rush-hour traffic. Secondly, the detachment of a coherent smoke layer from the ABL, starting at about 1400 LST (see Figure 6, top panel) corresponds to the onset of the decrease in the scattering coefficient in the early afternoon, as obtained from the nephelometer. Hence, this removal of aerosol through the top of the ABL affected the aerosol concentration throughout the boundary layer.

7. Discussion

It has been shown how forest-fire smoke can, under particular, yet not unusual, synoptic atmospheric conditions, substantially affect air quality and regional climate in regions remote from the fire origin. In the Québec forest-fire event of July 7, 2002, in Baltimore, the interplay of smoke that is advected by synoptic winds, large-scale subsidence and boundary-layer entrainment is responsible for high particle concentrations throughout the ABL, down to the ground. The smoke event presented a unique opportunity to study ABL characteristics using lidar.

Reflection and absorption of sunlight by a dense elevated smoke layer acted to lower daytime air temperature and possibly strengthen the ABL inversion. This contrasts with the regular case, where direct heating by shortwave radiation absorbed by aerosols *within* the boundary layer is found to be an important component of the boundary-layer heat budget (Angevine et al., 1998b). However, if larger amounts of aerosol are present in the atmosphere, the opposite can occur, as was shown here and elsewhere (Robock, 1988a, b; Menon et al., 2002), with implications for regional scale climate.

A prime purpose of our study was to investigate the structure of the atmospheric boundary layer in great detail, using the smoke particles as tracers. Several mechanisms were observed, such as dry convection, mixing inside the ABL, entrainment, and detrainment. We would like to note that detrainment, as observed in our study, differs greatly from detrainment observed for slope flows under stable atmospheric conditions (Monti et al., 2002), or in laboratory experiments (Fernando et al., 2001). In those cases, fluid can peel off as it flows upslope or downslope. As was shown by the lidar data time series taken during the haze event, pockets of boundary-layer air can overshoot the top of the ABL and break away under convective conditions.

Internal gravity waves can be excited in the non-turbulent region above the ABL by penetrative convection (Stull, 1976b). Our analysis (see Figure 7) confirms that disturbances, caused by overshooting thermals, can propagate vertically upward, away from the ABL.

There are some similarities between a cloud-topped boundary layer and the ABL on July 7, 2002, which was initially topped by a smoke layer. A smoke-topped ABL shares with the stratocumulus-topped ABL the essential features of turbulence and entrainment driven by radiative cooling (Moeng et al., 1999). The forest-fire smoke layer caused strong absorption of solar shortwave radiation due to black carbon ('soot'), which is re-emitted as longwave radiation, leading to radiative cooling. Shortwave radiation can also be simply reflected back to space (e.g., by non-absorbing particles such

as organic carbon). In a large-eddy simulation study of the ABL driven by smoke-cloud-top radiative cooling only (hence not fully comparable to the convectively driven ABL here) by Moeng et al. (1999), it was found that the entrainment rate depends substantially on the jump in longwave radiative flux above the entrainment buoyancy flux level. Furthermore, the radiative flux divergence was found to exist solely within the smoke region, which cools the smoke-cloud layer and thus enhances the local inversion strength. Noteworthy here is the study by Robock (1988b) who found that forest-fire smoke trapped in a valley strengthened the inversion by preventing surface warming due to solar radiation, thereby enhancing the smoke trapping and surface cooling in a positive feedback loop. These studies explain, in part, the strong lid effect of the smoke layer found here. In addition, they provide a physical explanation for the tremendously energetic wisps that carry large amounts of aerosol downward. These wisps originate within the entrainment zone, perhaps cooled due to radiative effects, and hence the EZ air mass becomes negatively buoyant, promoting energetic downward transport. Furthermore, note that the process of detachment might have been caused in part by differential absorption of sunlight. In an analogy to studies on the stratocumulus-topped ABL (e.g., Slingo et al., 1982; Driedonks and Duynkerke, 1989; Moeng, 1998) it appears that shortwave radiative heating (positive buoyant forcing) and longwave cooling (negative buoyant forcing) destabilised the smoke layer and led to detachment.

The smoke layer was initially above the ABL and intersected with the growing ABL due to subsidence. Since the process can be viewed as a type of fumigation, it is reasonable to compare the results with the study by Deardorff and Willis (1982). They found that the ground-level concentration was maximal 1–2 h after the fumigation process began. In the current study the start of fumigation is around 1140 LST, and the maximum scattering coefficient from the nephelometer was measured during the sampling interval 1330–1335 LST. Thus, a time lag of about 2 h is observed, which compares well with the result of Deardorff and Willis. Furthermore, the lidar visualisations show that wisps do not initially reach the ground; hence the fumigant is intercepted spottily by the mixed layer, producing the time lag, in agreement with Deardorff and Willis.

Acknowledgements

The authors wish to thank Mariana Adam, Chad Higgins, Elie Bou-Zeid and Vijayant Kumar (Johns Hopkins University) for their assistance in the field. We gratefully acknowledge the loan of equipment by Prof. Phil Hopke (Clarkson University). We would also like to thank the MODIS Land Rapid Response Team (NASA/GSFC, Greenbelt, Maryland) for permission to use

MODIS images. This research has been supported by the U.S. Environmental Protection Agency (EPA 99-NCERQA-X1).

References

Albertson, J. D. and Parlange, M. B.: 1999, 'Surface Length Scales and Shear Stress: Implications for Land-Atmosphere Interaction over Complex Terrain', *Water Resour. Res.* **35**, 2121–2132.

Angevine, W. M., Grimsdell, A. W., Hartten, L. M., and Delany, A. C.: 1998a, 'The Flatland Boundary Layer Experiment', *Bull. Amer. Meteorol. Soc.*, **79**, 419–431.

Angevine, W. M., Grimsdell, A. W., McKeen, S. A., and Warnock, J. M.: 1998b, 'Entrainment Results from the Flatland Boundary Layer Experiments', *J. Geophys. Res.* **103**, 13689–13701.

Deardorff, J. W. and Willis, G. E.: 1982, 'Ground-level Concentrations Due to Fumigation into an Entraining Mixed Layer', *Atmos. Environ.* **16**, 1159–1170.

Deardorff, J. W., Willis, G. E., and Lilly, D. K.: 1969, 'Laboratory Investigation of Nonsteady Penetrative Convection', *J. Fluid Mech.* **35**, 7–31.

Deardorff, J. W., Willis, G. E., and Stockton, B. H.: 1980, 'Laboratory Studies of the Entrainment Zone of a Convectively Mixed Layer', *J. Fluid Mech.* **100**, 41–64.

Driedonks, A. G. M. and Duynkerke, P. G.: 1989, 'Current Problems in the Stratocumulus-topped Atmospheric Boundary Layer', *Boundary-Layer Meteorol.* **46**, 275–303.

Fedorovich, E. and Thäter, J.: 2002, 'A Wind Tunnel Study of Gaseous Tracer Dispersion in the Convective Boundary Layer Capped by a Temperature Inversion', *Atmos. Environ.* **36**, 2245–2255.

Fernando, H. J. S., Lee, S. M., Anderson, J, Princevac, M., Pardyjak, E., and Grossmann-Clarke, S.: 2001, 'Urban Fluid Mechanics: Air Circulation and Contaminant Dispersion in Cities', *Environ. Fluid Mech.* **1**, 107–164.

Fochesatto, G. J., Drobinski, P., Flamant, C., Guedalia, D., Sarrat, C., Flamant, P. H., and Pelon, J.: 2001, 'Evidence of Dynamic Coupling between the Residual Layer and the Developing Convective Boundary Layer', *Boundary-Layer Meteorol.* **99**, 451–464.

Forster, C., Wandinger, U., Wotawa, G., James, P., Mattis, I., Althausen, D., Simmonds, P., O'Doherty, S., Jennings, S. G., Kleefeld, C., Schneider, J., Trickl T., Kreipl, S., Jager, H., and Stohl A.: 2001, 'Transport of Boreal Forest Fire Emissions from Canada to Europe', *J. Geophys. Res.* **106**, 22887–22906.

Garratt, J. R.: 1992, *The Atmospheric Boundary Layer*, Cambridge University Press, Cambridge, U.K., 316 pp.

Gossard, E. and Richter, J. H.: 1970, 'The Shape of Internal Waves of Finite Amplitude from High Resolution Radar Sounding of the Lower Atmosphere', *J. Atmos. Sci.* **27**, 971–973.

Iziomon, M. G. and Lohmann, U.: 2003, 'Optical and Meteorological Properties of Smoke-dominated Haze at the ARM Southern Great Plains Central Facility', *Geophys. Res. Lett.* **30**, doi:10.1029/2002GL016606.

Menon, S., Hansen, J., Nazarenko, L., and Luo, Y.: 2002, 'Climate Effects of Black Carbon Aerosols in China and India', *Science* **297**, 2250–2253.

Menut, L., Flamant, C., Pelon, J., and Flamant, P. H.: 1999, 'Urban Boundary-Layer Height determination from Lidar Measurements over the Paris Area', *Appl. Opt.* **38**, 945–954.

Metcalf, J. I.: 1975, 'Gravity Waves in a Low Level Inversion', *J. Atmos. Sci.* **32**, 351–361.

Moeng, C.-H.: 1998, 'Stratocumulus-Topped Atmospheric Planetary Boundary Layer', in E. J. Plate et al. (eds.), *Buoyant Convection in Geophysical Flows*, NATO Science Series C, Vol. 513, Kluwer Academic Publishers, Dordrecht, pp. 421–440.

Moeng, C.-H., Sullivan, P. P., and Stevens, B.: 1999, 'Including Radiative Effects in an Entrainment Rate Formula for Buoyancy-Driven PBLs', *J. Atmos. Sci.* **56**, 1031–1049.

Monti, P., Fernando, H. J. S., Princevac, M., Chan, W. C., Kowalewski, T. A., and Pardyjak, E. R.: 2002, 'Observations of Flow and Turbulence in the Nocturnal Boundary Layer over a Slope', *J. Atmos. Sci.* **59**, 2513–2534.

Pahlow, M.: 2002, *Atmospheric Boundary-Layer Dynamics and Inversion Technologies to Obtain Extinction Coefficient Profiles in the Atmosphere from Elastic Lidar*, Ph.D. Dissertation, Johns Hopkins University, Baltimore, MD, U.S.A., 209 pp.

Robock, A.: 1988a, 'Enhancement of Surface Cooling Due to Forest Fire Smoke', *Science* **242**, 911–913.

Robock, A.: 1988b, 'Surface Temperature Effects of Forest Fire Smoke Plumes', in P. V. Hobbs and M. P. McCormick (eds.), *Aerosols and Climate*, Deepak Publishing, Hampton, VA, pp. 435–442.

Scorer, R. S.: 1957, 'Experiment on Convection of Isolated Masses of Buoyant Fluid', *J. Fluid Mech.* **2**, 583–594.

Sigler, J. M., Lee, X., and Munger, W.: 2003, 'Emission and Long-Range Transport of Gaseous Mercury from a Large-Scale Canadian Boreal Forest Fire', *Environ. Sci. Technol.* **37**, 4343–4347.

Skinner, W. R., Flannigan, M. D., Stocks, B. J., Martell, D. L., Wotton, B. M., Todd, J. B., Mason, J. A., Logan, K. A., and Bosch, E. M.: 2002, 'A 500 hPa Synoptic Wildland Fire Climatology for Large Canadian Forest Fires, 1959–1996', *Theor. Appl. Climatol.* **71**, 157–169.

Skinner, W. R., Stocks, B. J., Martell, D. L., Bonsal, B., and Shabbar, A.: 1999, 'The Association between Circulation Anomalies in the Mid-Troposphere and Area Burned by Wildland Fire in Canada', *Theor. Appl. Climatol.* **63**, 89–105.

Slingo, A., Nicholls, S., and Schmertz, J.: 1982, 'Aircraft Observations of Marine Stratocumulus during JASIN', *Quart. J. Roy. Meteorol. Soc.* **108**, 833–856.

Stull, R. B.: 1976a, 'The Energetics of Entrainment across a Density Interface', *J. Atmos. Sci.* **33**, 1260–1267.

Stull, R. B.: 1976b, 'Internal Gravity Waves Generated by Penetrative Convection', *J. Atmos. Sci.* **33**, 1279–1286.

Stull, R. B.: 1988, *An Introduction to Boundary Layer Meteorology*, Kluwer Adademic Publishers, Dordrecht, 666 pp.

Sullivan, P. P., Moeng, C.-H., Stevens, B., Lenshow, D. H., and Mayor, S. D.: 1998, 'Structure of the Entrainment Zone Capping the Convective Atmospheric Boundary Layer', *J. Atmos. Sci.* **55**, 3042–3064.

Weber, M. G. and Stocks, B. J.: 1998, 'Forest Fires and Sustainability in the Boreal Forests of Canada', *Ambio* **27**, 545–550.

Wotawa, G. and Trainer, M.: 2000, 'The Influence of Canadian forest Fires on Pollutant Concentrations in the United States' *Science* **288**, 324–328.

Wyngaard, J. C. and Brost, R. A.: 1984, 'Top-Down and Bottom-Up Diffusion of a Scalar in the Convective Boundary Layer', *J. Atmos. Sci.* **41**, 102–112.

Yi, C., Davis, K. J., Berger, B. W., and Bakwin, P. S.: 2001, 'Long-Term Observations of the Dynamics of the Continental Planetary Boundary Layer', *J. Atmos. Sci.* **58**, 1288–1299.